DOE/PC/70768--9

DE92 000204

TECHNICAL PROGRESS REPORT

KINETICS OF COAL PYROLYSIS AND DEVOLATILIZATION

For the period January 1, 1987 - March 31, 1987

Work Performed under Contract No. DE-AC22-84PC70768

For

U. S. Department of Energy
Pittsburgh Energy Technology Center
P.O. Box 10940
Pittsburgh, PA 15236

By

United Technologies Research Center
East Hartford, CT 06108

INTRODUCTION

The objective of these experimental and modeling studies is to develop an improved understanding of the kinetics of coal devolatilization which is relevant to suspension firing of powdered coal. These fundamental kinetic studies address several topics related to pulverized coal combustion and include both homogeneous and heterogeneous reactions. The principal topics include: (a) the pyrolysis and devolatilization of coal; and (b) the formation of char. Research activities include small-scale experimentation, interpretation of experimental results in terms of mechanistic understanding and the developement and validation of kinetic models of fundamental processes.

This report consists of two contributions. The first is from MIT entitled "Intra-Particle Heat Transfer Effects in Coal Pyrolysis". While this modeling study bears some similarity to the Ohio State work, it is proposed as the starting point for a more complete model which will include other boundary conditions as well as mass transfer effects.

The second contribution is a report from UTRC entitled "Effect of Heat Transfer on Tar and Light Gases From Coal Pyrolysis". This work documents some of the changes in the chemical composition of the products of pyrolysis when the mode or rate of heat transfer is varied.

INTRA-PARTICLE HEAT TRANSFER EFFECTS IN COAL PYROLYSIS

Mohammed R. Hajaligol
William A. Peters
Jack B. Howard

Energy Laboratory and
Department of Chemical Engineering

M.I.T.
Cambridge, MA 02139

Introduction. Many coal combustion and gasification processes involve particle sizes and surface heating rates producing temporal and spatial temperature gradients within the coal particles during pyrolysis. These gradients may strongly influence volatiles yields, compositions, and release rates, and can confound attempts to model coal pyrolysis kinetics with purely chemical rate expressions. Mathematical modeling of particle non-isothermalities is needed to predict reaction conditions (viz., particle dimension, surface heating rate, final temperature, and reaction time) for which intra-particle heat transfer limitations do not significantly influence pyrolysis kinetics, and to predict pyrolysis behavior when they do. When pyrolysis is not thermal-neutral, the analysis is non-trivial since local temperature fields are coupled non-linearly to corresponding local heat release (or absorption) rates and hence to local pyrolysis kinetics.

Much of the pertinent literature has addressed pseudo steady-state models for spatial temperature gradients within catalyst particles playing host to endo- or exothermic reactions, including, for some cases, mathematical treatment of the attendant limitations on intra-particle mass transfer of reactants or products [See Ref. (1) and references cited therein]. There appear to have been few analyses of non-isothermalities within a condensed phase material simultaneously undergoing non-thermally neutral chemical reaction(s). Previous work includes rather empirical approaches to fitting coal weight loss kinetics [see reviews by Howard (2) and Gavalas (3)], and more refined analyses of spatial non-isothermalities within exploding solids (4,5). Gavalas (2) calculated regimes of coal particle size where pyrolysis kinetics should be free of heat transfer effects, and Simmons (6) provided similar information for cellulose pyrolysis. Valuable contributions are also

emanating from the laboratories of Essenhigh (7), and Freihaut and Seery (8).

There is need for a generic, quantitative formalism to reliably predict transient intra-particle non-isothermalities and their effects on pyrolysis, as a function of operating conditions of interest in modern fuels utilization technologies. To this end the present paper presents, for an isolated spherical coal particle pyrolyzing by a single first-order reaction, quantitative predictions of three distinct indices of particle non-isothermality - namely the extent of agreement between: (1) temperatures at the particle surface and centerline; (2) the pyrolysis rate [or (3) the pyrolysis weight loss] averaged over the particle volume and the corresponding quantity calculated using the particle surface temperature for the entire particle volume. Each index is explicitly dependent on time and thus accounts for the temporal as well as the spatial non-idealities in particle "isothermality".

Method of Analysis. Spatial limitations allow only a brief summary of the theoretical approach, which is described in more detail with broader applications, by Hajaligol et al. (9). For an isolated spherical coal particle with temperature invarient thermal physical properties, pyrolyzing by a single first-order endo or exo-thermic reaction with an Arrhenius temperature dependency, heated at its surface, and transmitting heat internally only by conduction, (or by processes well-described by an apparent isotropic thermal conductivity) a standard heat balance gives the following partial differential equation for the time and spatial dependence of the intra-particle temperature field

$$\frac{1}{\alpha}\left(\frac{\partial T}{\partial t}\right) = \frac{1}{r^2}\frac{\partial}{\partial r}\left(r^2\frac{\partial T}{\partial r}\right) + \frac{(-\Delta H_{py})\,\rho k_0\, e^{-E/RT}}{\lambda} \qquad (1)$$

Following Boddington et al. (1982) and others, this may be rewritten in dimensionless form as

$$\left(\frac{\partial \theta}{\partial \tau}\right) = \frac{1}{\xi^2}\frac{\partial}{\partial \xi}\left(\xi^2\frac{\partial \theta}{\partial \xi}\right) + \delta \exp\left[\frac{\theta}{\beta + \varepsilon\theta}\right] \qquad (2)$$

Symbols are defined in the nomenclature section at the end of the paper. Solution of Equation (1) or (2) requires specification of one initial condition and two spatial boundary conditions. The initial condition prescribes the temperature field throughout the coal particle at the instant heating begins

$$T(r,0) = T_o \qquad (3)$$

or

$$\theta(\xi,0) = 1 \qquad (4)$$

One boundary condition is the mathematical expression for centerline symmetry of the particle temperature field at all pyrolysis times

$$\left(\frac{\partial T}{\partial r}\right)_{r=0} = 0 \tag{5}$$

or

$$\left(\frac{\partial \theta}{\partial \xi}\right)_{\xi=0} = 0 \tag{6}$$

The four external surface boundary conditions most commonly used are:

(1) A finite rate of heat transmission to the particle surface describable in terms of an apparent heat transfer coefficient

$$-\lambda\left(\frac{\partial T}{\partial r}\right)_{r=R_0} = h_{eff}\left(T - T_\infty\right) \tag{7}$$

or

$$\left(\frac{\partial \theta}{\partial \xi}\right)_{\xi=1} = -N_{Bi}\left(\theta - \theta_\infty\right) \tag{8}$$

(2) A prescribed constant rate of increase in the particle surface temperature:

$$T_s(t) = T_0 + \dot{m}\, t \tag{9}$$

or

$$\theta_s(\tau) = 1 - \gamma\, \tau \tag{10}$$

(3) A known, constant surface heat flux density:

$$-\lambda\left(\frac{\partial T}{\partial r}\right)_{r=R_0} = \dot{q}/4\pi R_0^2 \tag{11}$$

or

$$\left(\frac{\partial \theta}{\partial \xi}\right)_{\xi=1} = -\Phi \tag{12}$$

(4) A special limiting case of (1) through (3) above is an infinitely rapid surface heating rate:

$$T_s(t) = T_s(\infty) \quad , \quad r = R_o \tag{13}$$

or

$$\Theta_s(\tau) = 0 \quad , \quad \xi = 1 \tag{14}$$

Equations (1) and (2) were solved numerically for each of the above four cases of boundary condition, using a procedure based on the method of lines and on Gear's method.

Case 1 is generally identified with reactors in which the main mode of heat transfer is across a fictitious film to the particle surface, such as fluid bed or low temperature entrained flow systems. Screen heater systems are generally assumed to create conditions in which boundary condition 2 is satisfied. Devolatilization induced by chopped laser beams or particle entrainment through a folded laser beam is generally represented by case 3. Case 4 is approximated by shock wave or dust explosion heating of suspended particles.

In practice, none of the four mathematical boundary conditions, as stated, adequately represent heat transfer conditions data. Developing a general understanding of coal devolatilization and a kinetic model requires experimentation in a wide range of reactor temperatures, a range of heat transfer modes, that is, irradiance versus conductive, and a range of particle residence times in the heating environment. Spatial and temporal resolution of any real heating environment is not infinite. Coupled radiation and conductive components are always present and their relative magnitudes vary considerably during the course of the particle response to the reactor heat transfer field, and, consequently, during the course of the devolatilization process. Linear, transient thermocouple responses in screen heaters are approached, but a number of assumptions are made in assigning the same linear response to the surface of coal particles in the same heat transfer field. The stated boundary conditions allow the mathematical determination of the sensitivity of particle temperature trajectories to varying idealized heating conditions and devolatilization processes.

The purpose of this investigation is to determine the sensitivity of the particle temperature trajectory to changes in assumed linear heating rate at the particle surface, case 2 above. Within these idealized heating conditions, the sensitivity of the transient particle temperature response and devolatilization to changes in kinetic parameters and heat of devolatilization is also examined.

The solutions to these two equations are predictions of the spatial variation of the intra-particle temperature field with pyrolysis time. This information was used to compute three distinct indices of particle non-isothermality:

(1) The extent of agreement between the surface and centerline temperature of the particle:

$$\eta_T(t) = \left[T_s(t) - T_{cL}(t)\right] \Big/ T_s(t) \tag{15}$$

or

$$\hat{\eta}(\tau) = \theta_{cL}(\tau) - \theta_s(\tau) \tag{16}$$

(2) A time dependent effectiveness factor for pyrolysis rate, defined as the ratio of: the local pyrolysis rate averaged over the particle volume, to the pyrolysis rate calculated using the particle surface temperature for the entire particle volume:

$$\eta_r(t) = \frac{\frac{1}{V}\int_V k_0 e^{-E/RT(V,t)}\, dV}{k_0 e^{-E/R\,T_s(t)}} \tag{17}$$

or

$$\hat{\eta}_r(\tau) = \frac{3\int_0^1 k_0 e^{-\frac{\beta}{\beta\varepsilon + \varepsilon^2\theta(\xi,\tau)}}\, \xi^2\, d\xi}{k_0 e^{-\beta/(\beta\varepsilon + \varepsilon^2\theta_s(\tau))}} \tag{18}$$

(3) A time-dependent effectiveness factor for overall pyrolytic conversion (i.e., weight loss or total volatiles yield) defined as the ratio of: the volume averaged weight loss, to the weight loss calculated using the particle surface temperature for the entire particle volume.

$$\eta_c(t') = \frac{1 - \frac{1}{V}\int_V \left\{ \exp\left[-\int_0^{t'} k_0 \, e^{-E/RT(V,t)} \, dt \right] \right\} dV}{1 - \left\{ \exp\left[-\int_0^{t'} k_0 \, e^{-E/RT_s(t)} \, dt \right] \right\}} \qquad (19)$$

or

$$\hat{\eta}_c(\tau') = \frac{1 - 3\int_0^1 \left\{ \exp\left[-\int_0^{t'} \phi \, e^{-\beta/[\varepsilon\beta + \varepsilon^2\theta(\xi,\tau)} \, d\tau \right] \right\} d\xi}{1 - \left\{ \exp\left[-\int_0^{t'} \phi \, e^{-\beta/[\varepsilon\beta + \varepsilon^2\theta_s(\tau)} \, d\tau \right] \right\}} \qquad (20)$$

Results and Discussion. The above analysis was used with boundary condition (2) [constant surface heating rate] to predict effects of various pyrolysis parameters on $\eta_T(t)$, $\eta_R(t)$, and $\eta_c(t)$ as a function of pyrolysis time. Unless otherwise stated the following values of thermal physical and chemical properties of the coal were employed: ρ = 1.3 g/cm^3, λ = 0.0006 cal/cm-s-C, C_p = 0.4 cal/g-C, $\Delta H_{p,y}$ = 0 cal/g, $k_o = 10^{13}$ s^{-1}, and E = 50 kcal/g-mole. Effects of non-zero heats of pyrolysis are discussed later in the paper.

Figures 1 - 3 respectively show the effects of particle size on $\eta_T(t)$, $\eta_R(t)$, and $\eta_c(t)$, for a surface heating rate and final temperature of 10^4 C/s and 1000 C. For particle sizes > 50 μm, the time to relax internal temperature gradients [i.e. for $\eta_T(t)$ to decline from its maximum value to about zero] increases with roughly the square of particle diameter as expected. Initially the spatial non-idealities in temperature (Fig. 1) increased with increasing pyrolysis time, because the time for the surface to reach the final temperature [$T_{s,f}/m$] is much less than the particle thermal response time, and the intra-particle temperature field is unable to keep pace with the rapidly rising surface temperature. The magnitude and duration of this initial temperature transient increases with particle diameter, because the particle thermal response time increases with particle size.

The rate index of non-isothermality, $\eta_R(t)$ (Figure 2) tracks the non-idealities in particle temperature. For a given particle size and thermally neutral reactions $\eta_R(t)$ indicates spatially non-isothermal kinetic behavior [i.e. $\eta_R(t) < 1$] over a broader range of pyrolysis times than does $\eta_R(t)$ [i.e. for which $\eta_R(t) > 0$, Fig. 1]. The rate index expresses the influence of the temperature non-idealities on the predicted volume averaged pyrolysis rates via an exponential function. Thus an amplification of the magnitude and duration of the temperature non-idealities is not surprising. Furthermore, when volatiles release rates are of interest, $\eta_R(t)$ is clearly a more reliable index of particle non-isothermality than is $\eta_T(t)$.

The conversion index of non-isothermality, $\eta_c(t)$ (Fig. 3), reflects the non-idealities in rate, and the exponential increase in conversion with total pyrolysis time. The latter effect attenuates the former at short and long pyrolysis times by respectively, denying and supplying the reaction adequate time to attain completion at the imposed heating rate. Thus for each particle size there is an intermediate range of reactions times throughout which the strong non-idealities in pyrolysis rate (Fig. 2) contribute major non-idealit-

ies in conversion (Fig. 3). The exponential dependencies of conversion on rate and reaction time, also cause the magnitude of $\eta_c(t)$ to change rapidly with pyrolysis time, resulting in the sharp variations in this index depicted in Fig. 3. Clearly, in light of the differences in Figures 1 through 3, when total volatiles yield is of interest, $\eta_c(t)$ is the preferred index of non-isothermality over either $\eta_T(t)$ or $\eta_r(t)$.

Figure 4 shows that at a fixed particle size, increasing the surface heating rate increases the magnitude but decreases the duration of the initial non-idealities in the particle temperature field. The first effect arises because, with increasing surface heating rate, the surface temperature increases so rapidly during a time equal to the thermal response time of the particle, that the intra-particle temperature field lags further and further behind the surface temperature. The shorter relaxation time arises because the higher initial temperature gradients generated at higher surface heating rates cause a more rapid attenuation of the initial disturbance. With increasing heating rate, these sharp initial intra-particle temperature gradients translate into strong non-idealities in the local pyrolysis rates and hence into significant departures of $\eta_r(t)$ from unity (Fig. 5). With declining heating rates (Fig. 5) the magnitude of these non-idealities is attenuated but they remain significant over increasing ranges of pyrolysis time. These effects respectively arise because decreasing the surface heating rate reduces the differences between the surface and internal temperatures (Fig. 4), and because the resulting intra-particle temperature gradients are lower, and thus provide less driving force for temperature relaxation, thereby extending the time over which the intra-sample pyrolysis rates exhibit significant non-idealities. Increasing particle size at a fixed heating rate exacerbates each of the above effects (Fig. 2).

The impacts of these intra-sample rate variations on the conversion index of non-isothermality $\eta_c(t)$, are attenuated strongly in both magnitude and duration (Fig. 6), due to the interplay of rate and cumulative pyrolysis time discussed above. The magnitude of the non-idealities in $\eta_c(t)$ are worsened with increasing heating rate, because surface temperature and surface pyrolysis rate more and more rapidly outpace the corresponding quantities within the particle, thus expanding the differences between the extents of conversion predicted for these two regions at smaller and smaller reaction times. Conversely, the non-idealities in $\eta_c(t)$ decrease when heating rate decreases, because the particle temperature field (Fig. 4), and average pyrolysis rate (Fig. 5), track the surface temperature more and more closely, and because the greater time required for the surface temperature to attain its final value, allows intra-particle conversion to proceed further to completion.

For a thermally neutral reaction, a change in the activation energy for pyrolysis has no effect on intra-particle temperature gradients [and hence on $\eta_T(t)$], but Figure 7 shows that increasing E increases the magnitude of the non-idealities in $\eta_r(t)$, as would be expected since larger E's imply stronger dependencies of rate on temperature. Since $\eta_T(t)$ is unaffected by changing E, any effect of E on $\eta_c(t)$ will reflect only E-induced changes in $\eta_r(t)$. Such effects should be small since at this heating rate (10^3 C/s) quite large changes in $\eta_r(t)$ at an E of 50 kcal/g-mole (Fig. 5), are strongly attenuated in $\eta_c(t)$ (Fig. 6), and the E-induced variations in $\eta_r(t)$ (Fig. 7) are by comparison, rather small.

Figure 8 shows that for constant ρ and C_p, decreasing either the thermal conductivity or thermal diffusivity of the coal increases the magnitude and duration of non-idealities in $\eta_r(t)$ and $\eta_c(t)$. For an endothermic reaction the values of $\eta_T(t)$ and $\eta_r(t)$ at long pyrolysis times would increase with increasing values of either of these thermal parameters. For example, for ΔH_{py} = +50 cal/g coal, these two indices would increase by a factor of 10, for 10 to 15% increases in α or λ (Hajaligol et al. 1987).

Figure 9 shows the effects of pyrolysis time on $\eta_T(t)$, $\eta_r(t)$, and n(t) for cases where pyrolysis is not thermal neutral. The discussion is simplified by expressing the results in terms of a dimensionless parameter δ, which reflects the interaction of chemical kinetic and thermal physical parameters in determining the impact of chemical enthalpy on particle non-isothermality. Delta is derived by non-dimensionalizing Eq. (1), see Eq. (2), and physically can be thought of as the ratio of the average rate of heat generation (or depletion) at the particle surface from pyrolysis, to the average rate of conductive transfer of heat into the particle from its surface. Figure 9 shows that for reasonable exo- or endo-thermicities, $\eta_T(t)$ and $\eta_r(t)$ do not approach perfect ideality, even at long pyrolysis times, while $\eta_c(t)$ goes virtually to unity (isothermal behavior) in reasonable times. The magnitude and duration of the non-idealities expressed by $\eta_c(t)$ depend on the ratio of the pyrolysis time to the particle heat-up time (Hajaligol et al. 1987). At long pyrolysis times $\eta_T(t)$ and $\eta_r(t)$ attain δ-specific plateaus that are independent of heating rate or particle size, although both parameters affect the magnitude and duration of the transients in these two indices.

Figure 10 shows, for thermally neutral pyrolysis, domains of particle size and surface heating rate where the particle is at least 95% "isothermal" according to each of the above indices [$\eta_T(t)$, $\eta_r(t)$, and $\eta_c(t)$]. The temperature index provides a broader range of compliant particle sizes and heating rates, because it is uninfluenced by devolatilization kinetics. For a non-thermally-neutral reaction it is much more difficult to define domains of particle size and heating rate where $\eta_T(t)$ meets the 95% ideality criterion - note the very small δ values required for $\eta_T(t)$ to approach 0 in Fig. 9.

The rate index [$\eta_r(t)$] obviously enfolds kinetic effects, and consequently presents a more narrow domain of isothermality (Fig. 10). Clearly this index, rather than $\eta_T(t)$ alone, should be considered in evaluating the role of heat transfer effects in devolatization kinetic data and in designing experiments to probe intrinsic chemical rates. The conversion index, $\eta_c(t)$, provides a somewhat broader isothermality domain, due to the damping effect of pyrolysis time discussed above.

Effects of activation energy and thermal physical properties on the isothermality domains can be inferred from Fig.'s 7 and 8 respectively. Increasing or decreasing E as in Fig. 7, has no effect on the regions prescribed by $\eta_T(t)$ and $\eta_c(t)$, but respectively decreases and increases the domains defined by $\eta_r(t)$ (dashed lines of Fig. 10).

When pyrolysis is not thermally neutral, the domains of particle isothermality may, depending on the magnitude of ΔH_{py}, shrink from the boundaries defined in Fig. 10. Regimes of D_p and $\dot{m}$ meeting each of the above criteria can still be prescribed by calculating compliant families of curves in Fig. 10, using ΔH_{py} as a parameter. Alternatively, the parameter δ can be used to

advantage in a more efficient computation procedure that accounts explicitly for all parameters contributing to heat of pyrolysis effects. The rate index, $\eta_r(t)$ shows the greatest effect of $\Delta H_{p,y}$ (Fig. 9). Figure 11 shows how $\eta_r(t)$ varies with $|\delta|$, where the upper and lower branches [$\eta_r(t) > 1$, and < 1], reflect exo- and endo-thermic pyrolysis, respectively. This figure is used to obtain values of δ such that $\eta_r(t)$ indicates a desired extent of isothermality, say 95%. With δ fixed, and fixed thermal-physical properties, the particle diameter, D_p, final surface temperature T_s, and surface heating rate, m, become the only adjustable parameters of the system. For preselected particle diameters, Fig. 10 is then used to define the allowed maximum surface heating rates for any of the isothermality indices, and the value from Fig. 11 sets the corresponding maximum allowed surface temperature. Alternatively a desired surface heating rate can be pre-selected with the corresponding maximum allowed particle diameter and surface temperature being obtained from Figs. 10 and 11 (via δ) respectively, or a maximum surface temperature can be pre-chosen with the compliant δ value (Fig 11) prescribing the maximum allowed D_p, and Fig. 10 the corresponding maximum acceptable surface heating rate. This protocol is conservative in that it is valid for all pyrolysis times, and utilizes the most stringent of the above isothermality indices, $\eta_r(t)$.

Conclusions

1. The extent of coal particle non-isothermality at any stage of pyrolysis can be quantitatively depicted in terms of numerical indices reflecting not only spatial non-uniformities of the intra-particle temperature field, but also non-idealities in the rate and extent of pyrolysis.

2. Mathematical modeling of coupled rates of intra-particle pyrolysis and heat transmission, relates each index to operating conditions of interest in coal combustion and gasification including surface heating rate, particle diameter, final temperature, and pyrolysis time.

3. Domains of surface heating rate and particle diameter where each isothermality criterion is met to within 5% at all pyrolysis times are plotted for a base case of zero heat of pyrolysis.

4. Data and procedures for using these same isothermality maps when pyrolysis is not thermal neutral are also provided.

5. The analysis shows that diagnosing a pyrolyzing coal particle as "isothermal" based upon close agreement between its surface and centerline temperature, can lead to serious errors in estimates of corresponding volatiles release rates and total volatiles yields.

6. Each isothermality index exhibits significant temporal variations, showing that pyrolysis time, and hence extent of conversion must be considered in assessing particle non-isothermality and its impact on pyrolysis behavior.

Nomenclature

d_p	Particle Diameter, Cm
E	Activation Energy, Cal/g-mole
h_{eff}	Effective Heat Transfer Coefficient, Cal/(Cm²-Sec-C)
k_o	Reaction Frequency Factor, sec^{-1}
$\dot{m}$	Surface Heating Rate, °K/sec
N_{Bi}	Biot Number; $h_{eff}\, d_p / 2\lambda$
$\dot{q}$	Surface Heat Flux Density, Cal/sec
R	Gas Constant; 1.987 Cal/gmole°K
r	Radius, Cm
R_o	Partice Radius, Cm
T	Temperature, °K
T_o	Initial Temperature, °K
T_s	Surface Temperature, °K
$T_{s,f}$	Final Surface Temperature, °K
T_∞	Ambient Temperature, °K
t	Time, Sec
V	Particle Volume, Cm^3
ρ	Particle Density, g/cm^3
λ	Particle Thermal Conductivity, Cal/(Cm-Sec-C)
α	Particle Thermal Diffusivity, Cm^2/Sec
ΔH_{py}	Heat of Pyrolysis, Cal/g
Θ	Dimensionless Temperature; $\frac{T - T_{s,f}}{T_o - T_{s,f}}$
Θ_s	Dimensionless Surface Temperature; $\frac{T_{s(t)} - T_{s,f}}{T_o - T_{s,f}}$
Θ_{CL}	Dimensionless Center Temperature; $\frac{T_{CL(t)} - T_{s,f}}{T_o - T_{s,f}}$
Θ_∞	Dimensionless Ambient Temperature; $\frac{T_\infty - T_{s,f}}{T_o - T_{s,f}}$
τ	Dimensionless Time; $\alpha t / R_o^2$
ξ	Dimensionless Length; r/R_o

$\eta_T, \hat{\eta}_T$ Dimensionless Temperature Index

$\eta_r, \hat{\eta}_r$ Dimensionless Rate Index

$\eta_c, \hat{\eta}_c$ Dimensionless Conversion Index

ε Dimensionless Parameter; $R T_{s,f} / E$

β Dimensionless Parameter; $R T_{s,f}^2 / E (T_o - T_{s,f})$

δ Dimensionless Parameter; $(-\Delta H_{py}) \rho d_p^2 k_o e^{-E/R T_{s,f}} / [4 \lambda (T_o - T_{s,f})]$

γ Dimensionless Heating Rate; $\dot{m} d_p^2 / [4 \alpha (T_o - T_{s,f})]$

Φ Dimensionless Heat Flux Density; $\dot{q} / [2\pi \lambda d_p (T_o - T_{s,f})]$

Acknowledgements

Prime U.S.D.O.E. support for this work was provided via Contract No. DE-AC22-84PC70768, from the AR & TD Combustion Program of the Pittsburgh Energy Technology Center. Additional U.S.D.O.E. support was provided under Contract No. DE-AC21-85MC222049, from the Advanced Gasification Program of the Morgantown Energy Technology Center.

References

1. Froment, G. F., and K. B. Bischoff, Chemical Reactor Analysis & Design, John Wiley and Sons, 1979.

2. Howard, J. B., Fundamentals of Coal Pyrolysis and Hydropyrolysis, in Chemistry of Coal Utilization, 2nd Suppl. Vol., Wiley NY 1981.

3. Gavalas, G. R., Coal Pyrolysis, Elsevier Scientific Pub., 1982.

4. Boddington, T., P. Gray, and S. K. Scott, J. Chem. Soc., Faraday Trans. 2, 78, 1721-1730, 1982.

5. Scott, S. K., T. Boddington, and P. Gray, Chem. Eng. Science, Vol. 39, No. 6, 1079-1085, 1984.

6. Simmons, G.M., Am. Chem. Soc., Div. of Fuel Chem. Preprints, April 1984.

7. Essenhigh, R.H., Dept. of Mechanical Eng., Ohio State University, Work in Progress, 1987.

8. Seery, D. J., J. D. Freihaut, and W. M. Proscia, Technical Progress Reports for DOE, 1985-1986, United Technologies Research Center, E. Hartford, CT.

9. Hajaligol, M. R., J. B. Howard, and W. A. Peters, Predicting Temporal and Spatial Non-Isothermalities within Reacting Condensed Phase Media, To be Submitted to the AIChE journal, 1987.

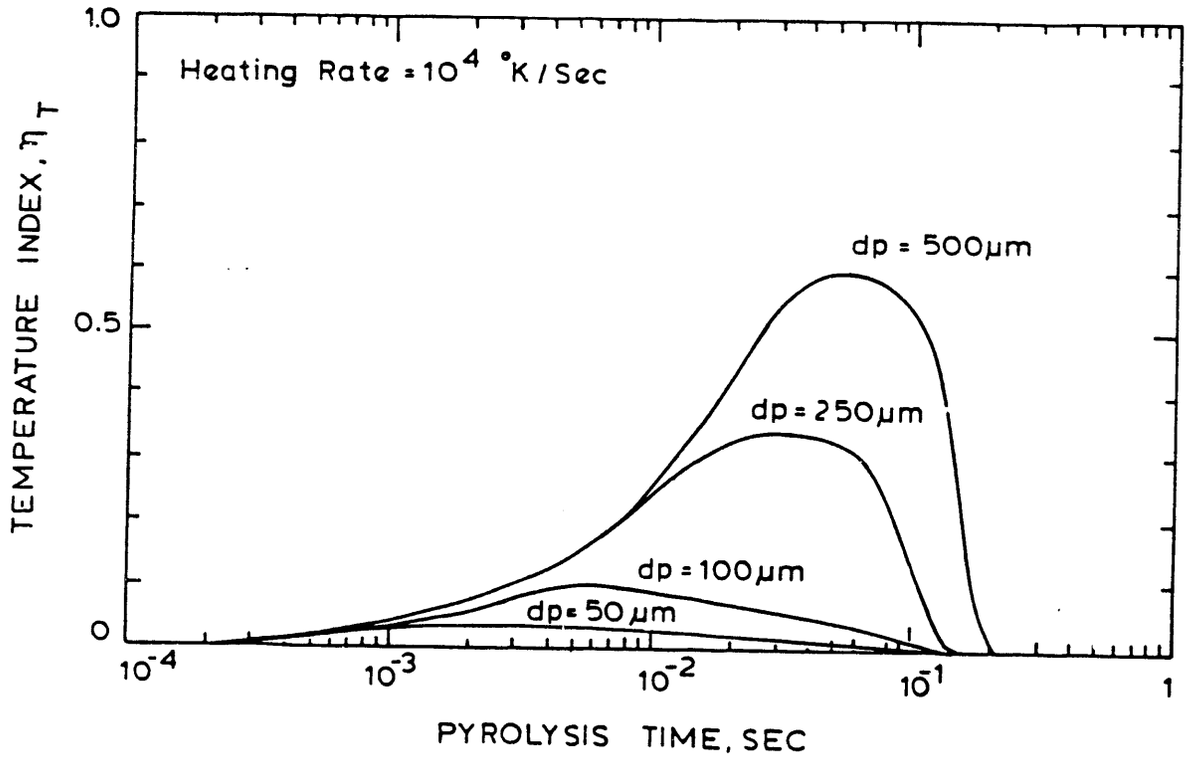

Figure 1. Effects of Particle Diameter on the Temperature Index at 10^4 K/sec Heating Rate.

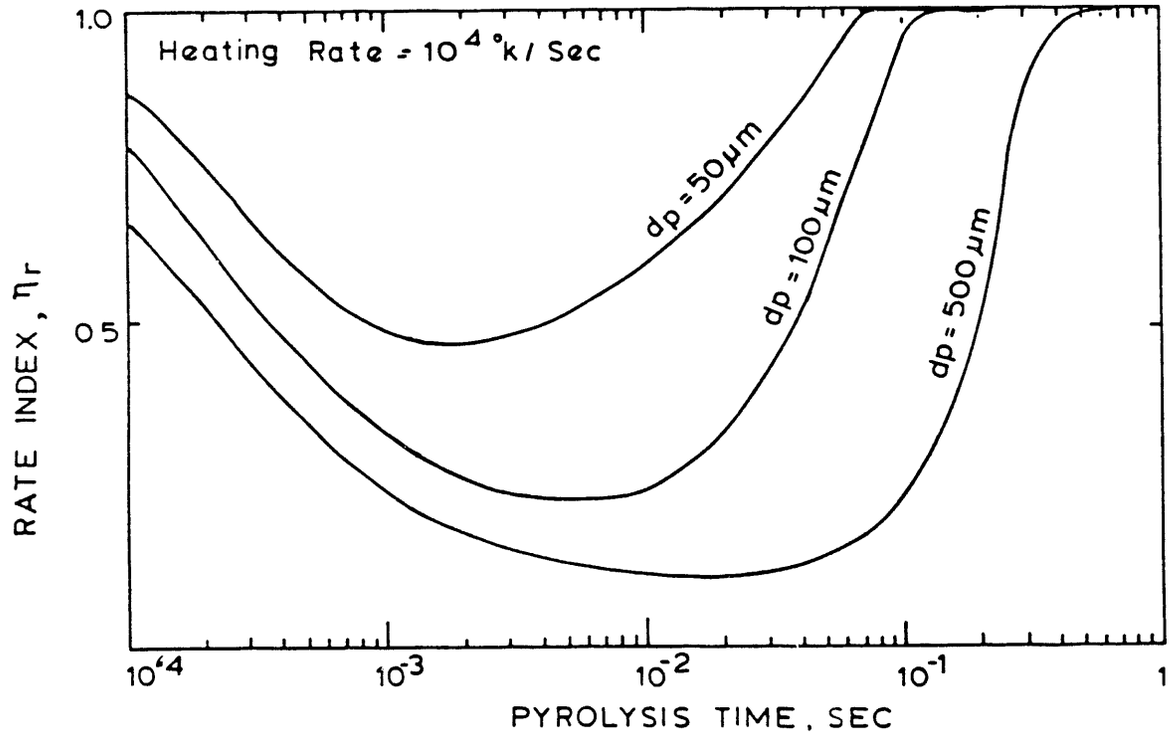

Figure 2. Effects of Particle Diameter on the Rate Index at 10^4 K/sec Heating Rate.

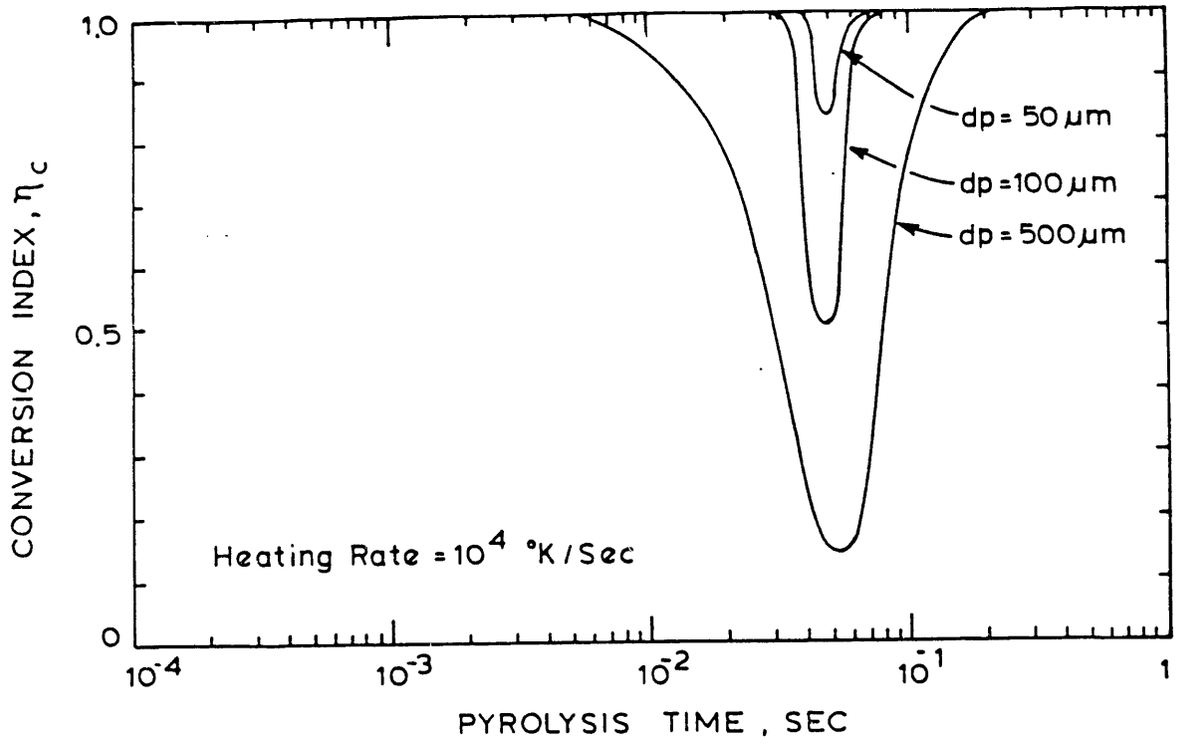

Figure 3. Effects of Particle Diameter on the Conversion Index at 10^4 K/sec Heating Rate.

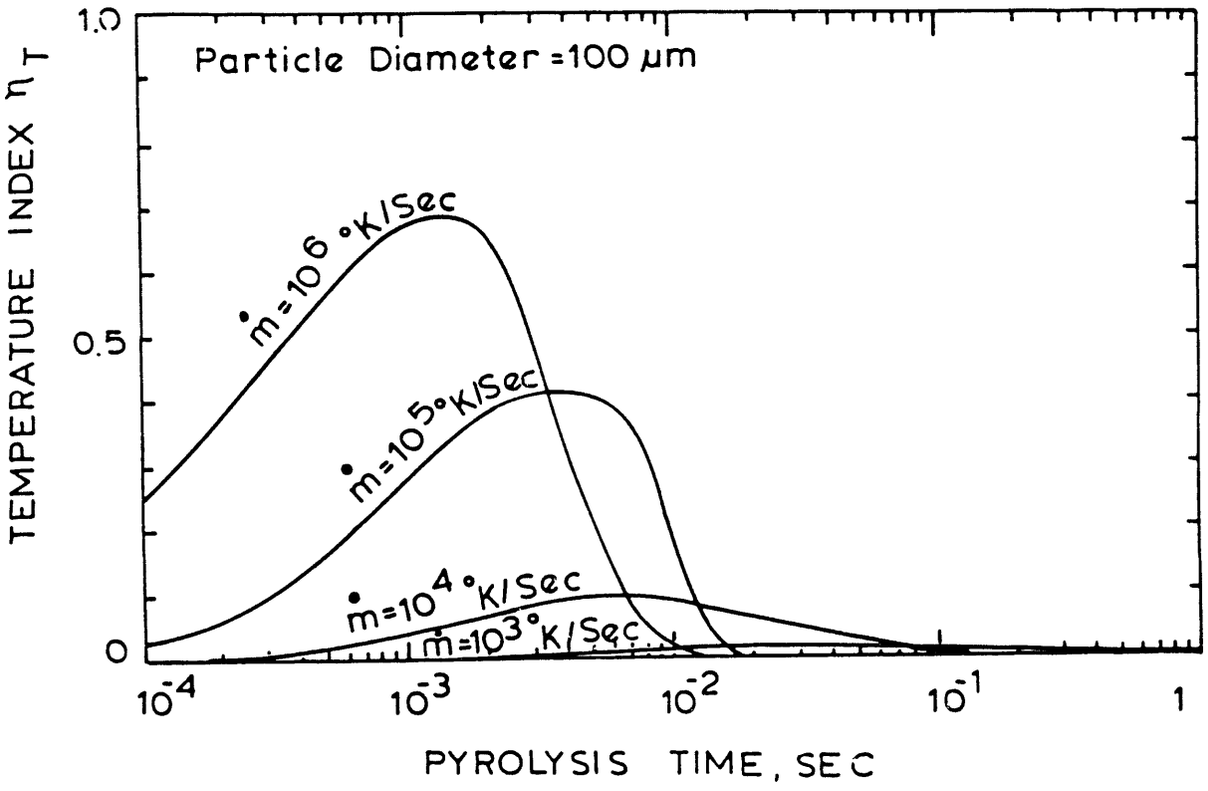

Figure 4. Effects of Heating Rate on the Temperature Index for 100 mm Particle Diameter.

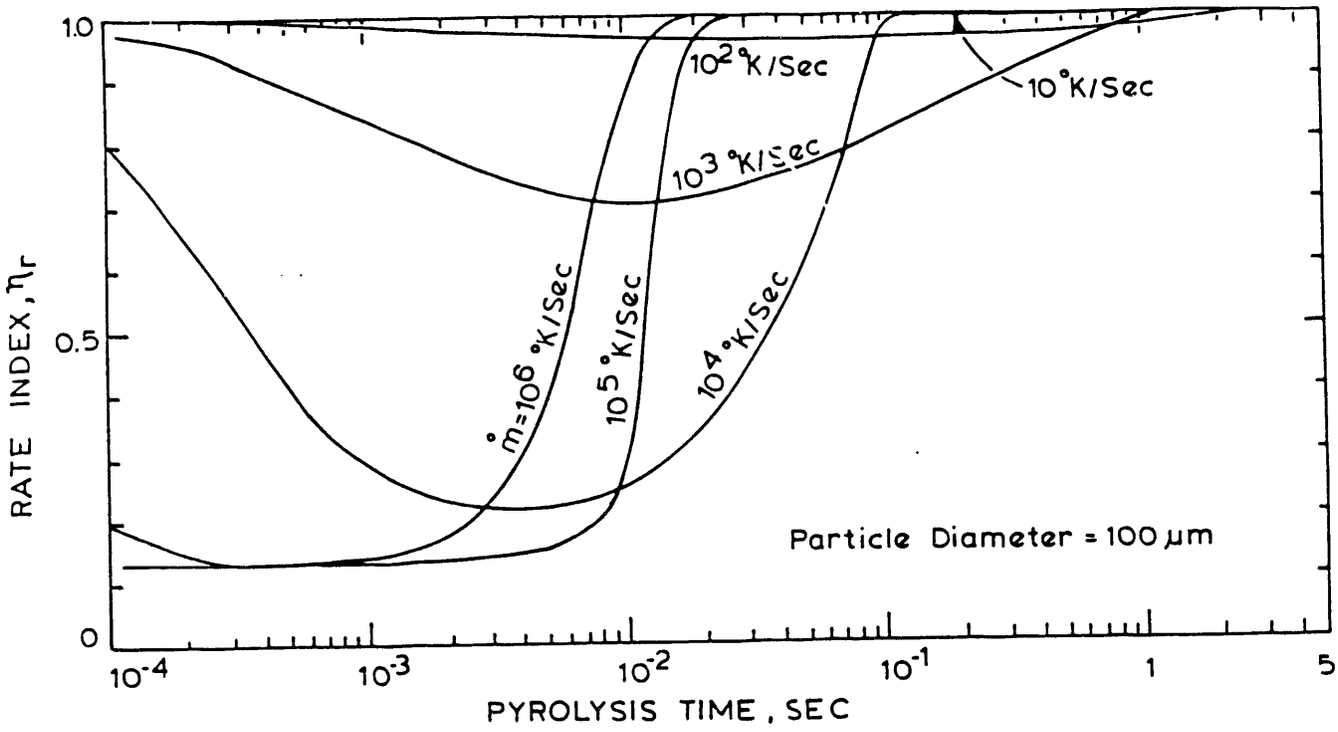

Figure 5. Effects of Heating Rate on the Rate Index for 100 mm Particle Diameter.

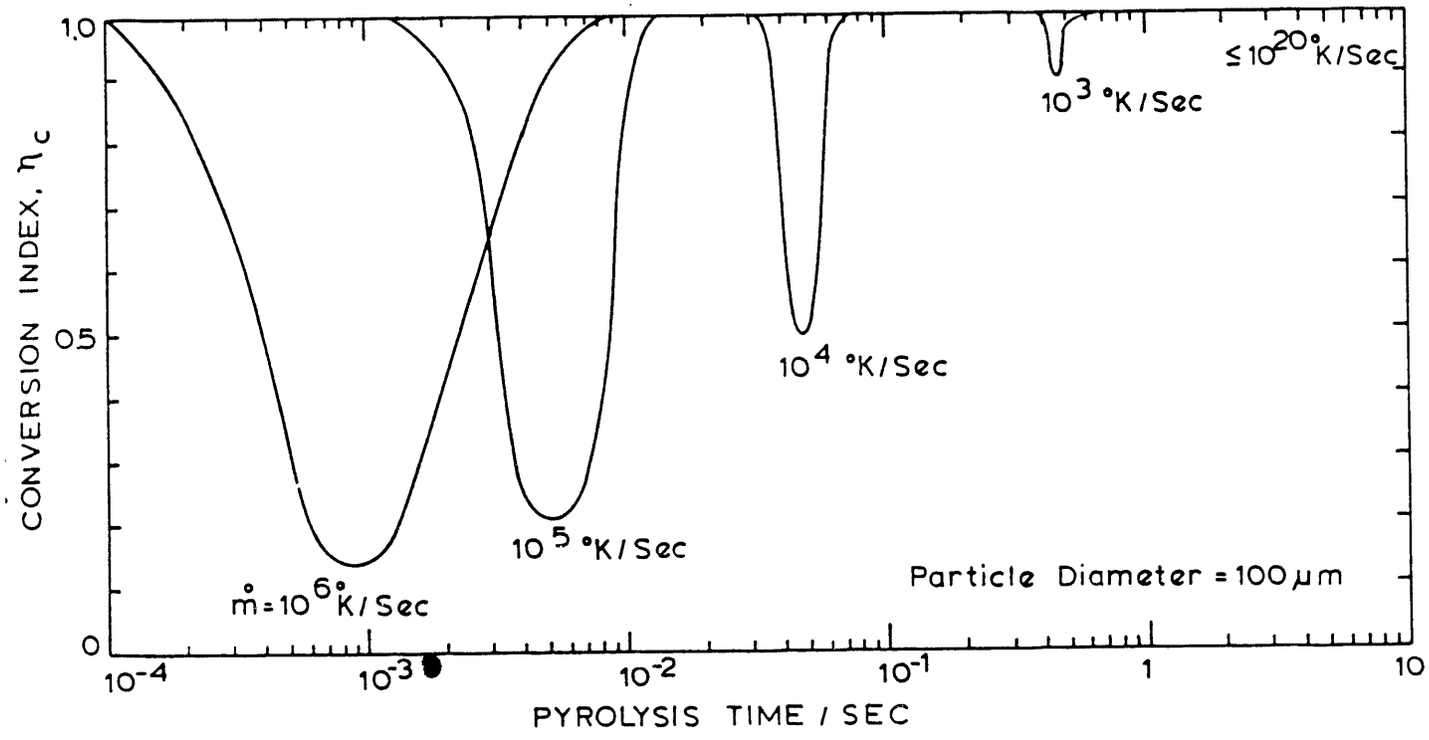

Figure 6. Effects of Heating Rate on the Conversion Index for 100 mm Particle Diameter.

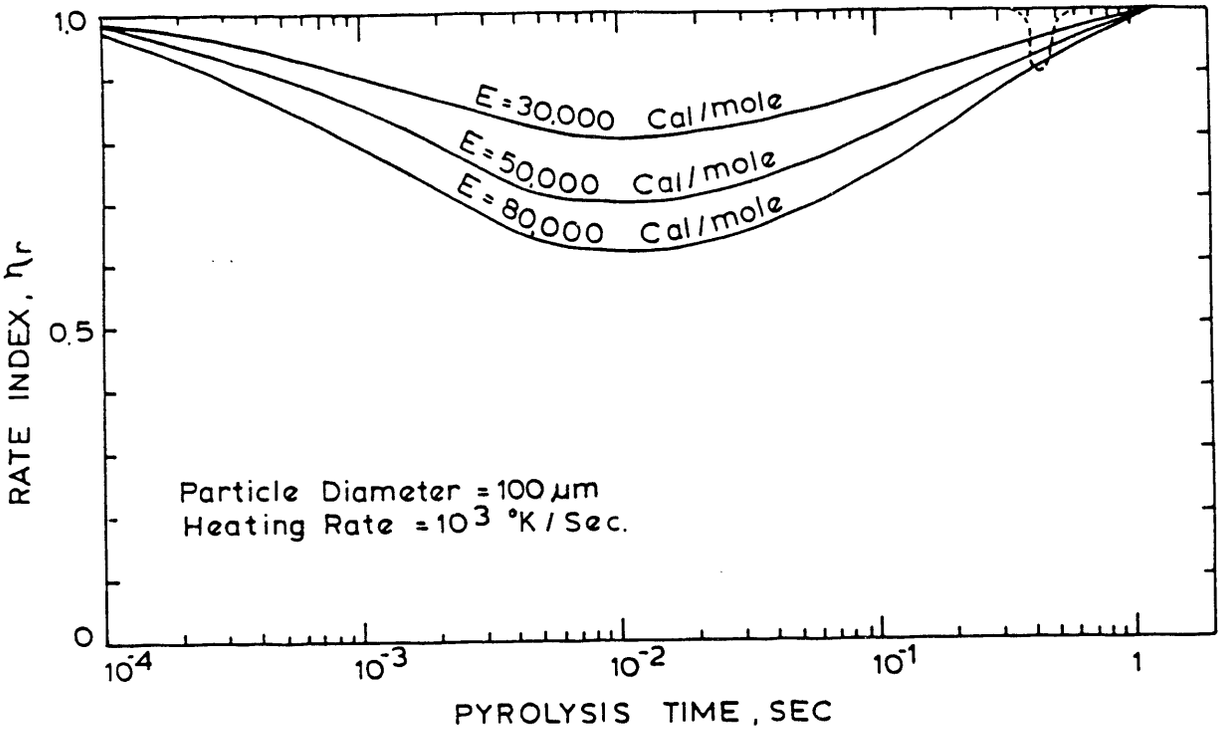

Figure 7. Effects of Activation Energy on the Rate and Conversion Indices.

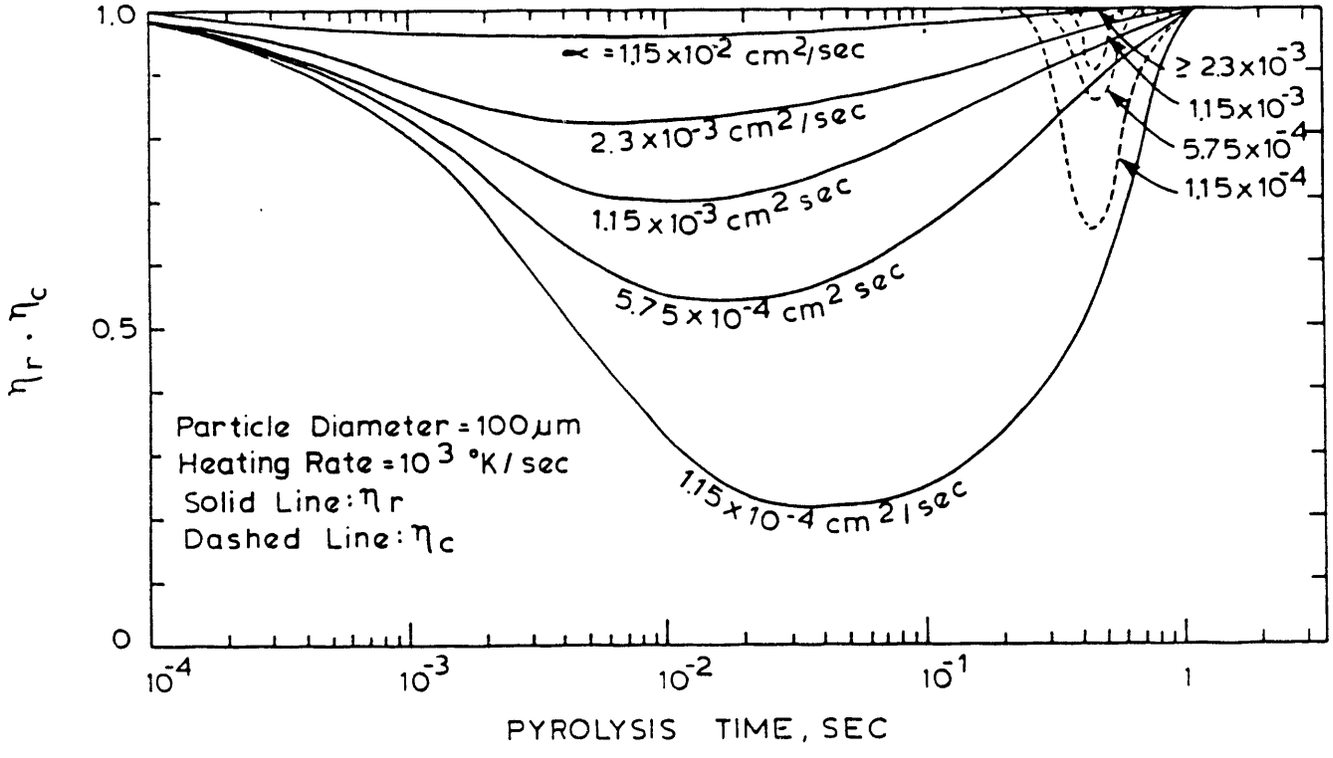

Figure 8. Effects of Thermal Diffusivity on Rate and Conversion Indices.

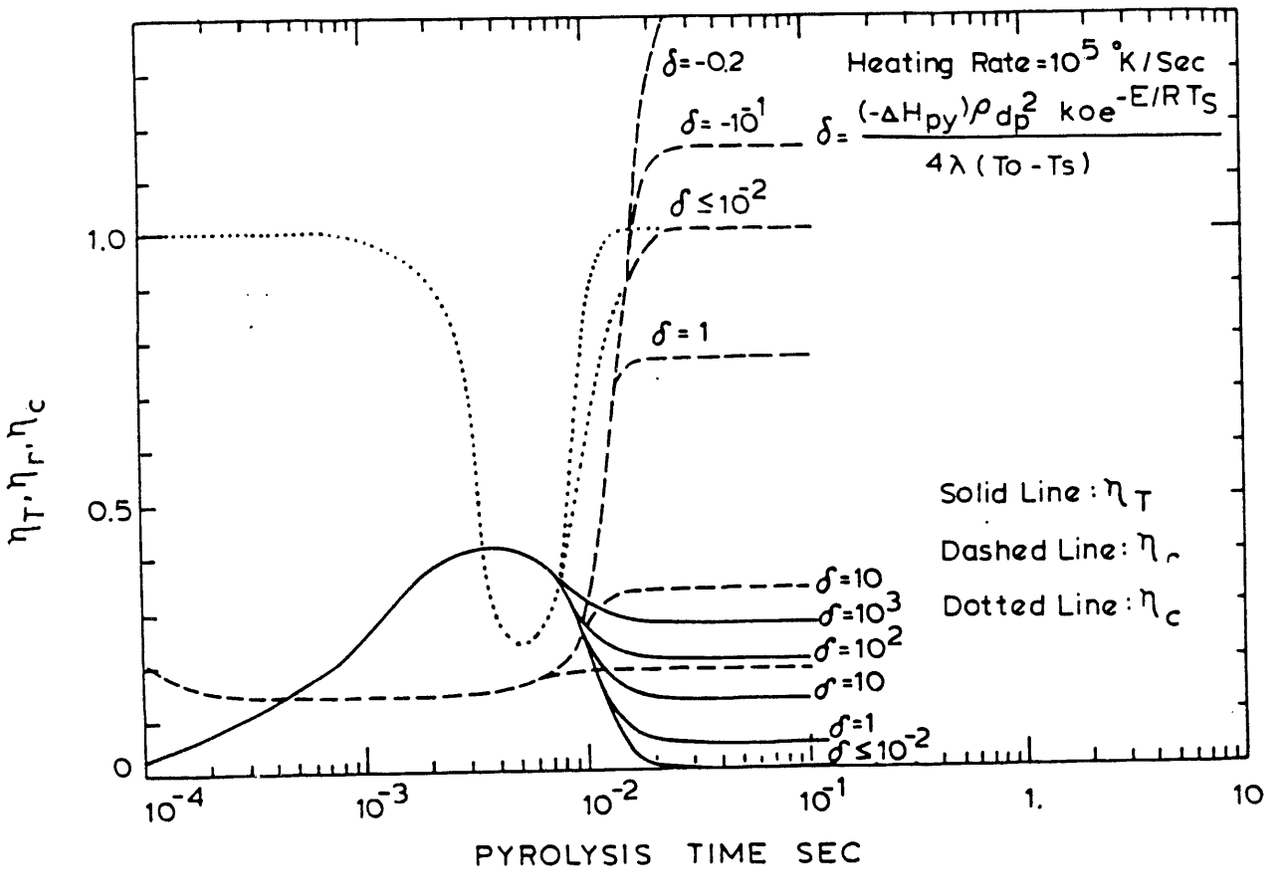

Figure 9. Effects of Heat of Pyrolysis on Indices.

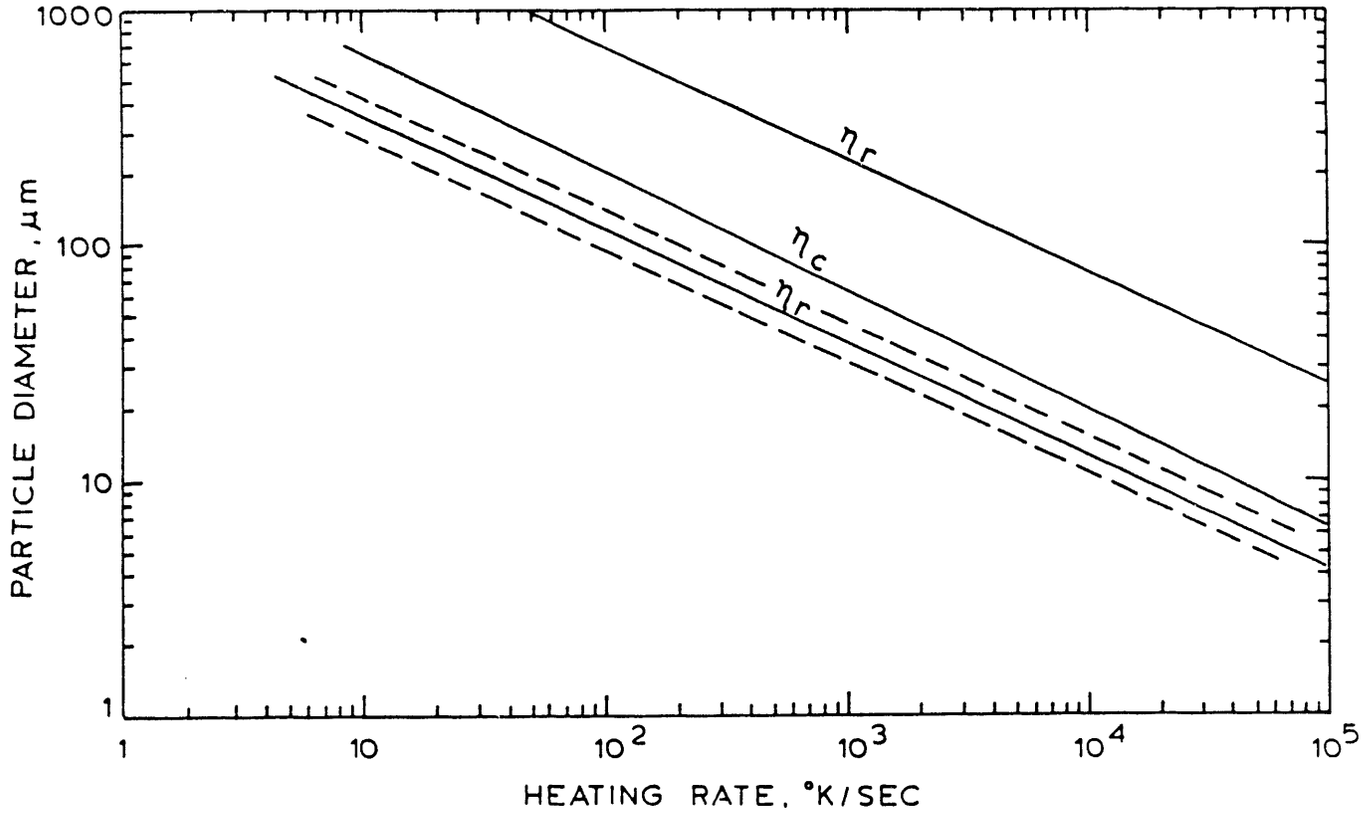

Figure 10. Isothermal Regions Defined by Different Indices.

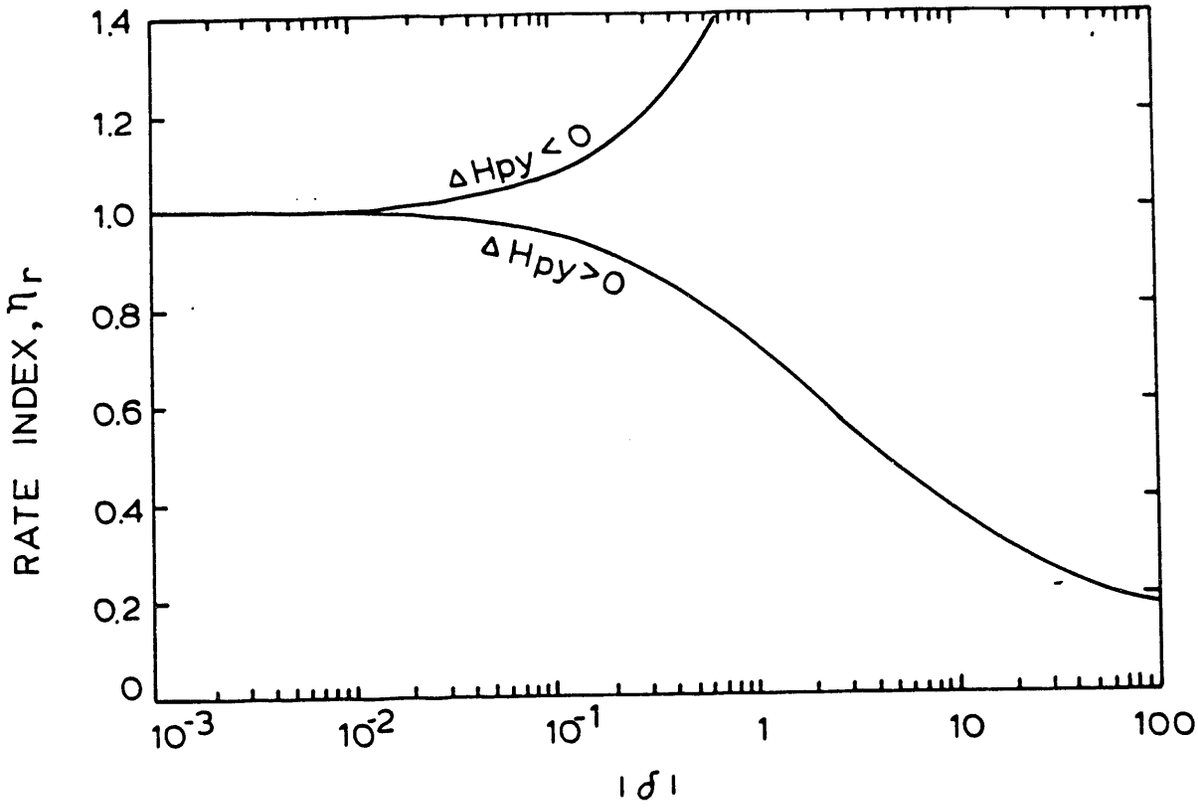

Figure 11. Effects of Heat of Pyrolysis on the Spatial Value of Rate Index.

EFFECT OF HEAT TRANSFER ON TAR AND LIGHT GASES FROM COAL PYROLYSIS

J. D. Freihaut
W. M. Proscia
D. J. Seery

United Technologies Research Center
East Hartford, CT 06108

Introduction: Recent evidence has demonstrated that the products of coal pyrolysis vary with the conditions of heating. Both the reactivity of the char and the chemical composition of the evolved species vary with thermal flux during pyrolysis. Because of the inherent complexity of coal, it is difficult to uncouple the actual heat transfer process and the effects of variations in individual parameters in most pyrolysis experimental designs. Typical ranges of heat transfer rates available in a number of devolatilization reactor systems are indicated in Fig. 1. A particular reactor system may have additional constraints imposed by the nature of the heat flux source or transfer media - acceptable particle size of the parent coal, ambient pressure in which devolatilization can be performed, spectral distribution of a radiant source, residence time in the heat transfer field, etc. Some practical size constraints of wire grid and entrained flow reactor systems are noted in Figure 1.

This report presents the results of a study of coal pyrolysis in three different reactors covering a wide range of heating conditions. The specific purpose of the investigation was to determine if the rate of heat delivery to a high volatile bituminous coal during the tar formation and evolution phase has a significant effect on the tar yields and molecular weight distribution for a high volatile bituminous coal. From the point of view of understanding coal devolatilization and the development of fundamental kinetic models, the investigation is geared to determining whether the same tar formation and evolution processes are occuring in widely different regimes of heat transfer rate and modes of heat transfer. The heavy hydrocarbons yields and chemical characteristics provide a type of observable monitor, to generate a microscopic model of the devolatilization/pyrolysis process.

EXPERIMENTAL

Reactor Characterization

The influence of transport on coal devolatilization necessitates the characterization of reactor heat transfer properties in detail. Figure 1 displays the power density regimes required for a given heating rate of inert, spherical particles having thermal capacities equivalent to coal. Also shown are the range of power density capabilities of the heated grid and flash lamp reactors employed in this investigation and the corresponding regimes for entrained flow reactors. The heated grid system employed in this investigation generates power densities of 1-6 watts/cm^2 at grid temperatures between 600°K and 1200°K. The flash lamp system generates power densities, in the form of transient irradiance levels. Time averaged levels from 200 watts/cm^2 to greater than 700 watts/cm^2 were employed. Entrained flow reactors generally operates in the 10-100 watts/cm^2 regime. Final particle

temperatures of 1000°K or greater can be obtained in each system, but for significantly different transient times.

UTRC Heated Grid (HG)

The heated grid experiments are conducted by imposing a controlled voltage across a folded No. 325 mesh stainless steel screen. The screens are prefired, then loaded with 20-30 mg of coal by evenly distributing the coal between the folds of the screen. Simultaneous, real time measurements of applied voltage across the screen, current flow, and temperature of the screen are made by a rapid data acquisition system. The grid, char and tar are quenched by impingement of high velocity helium jets on the grid at the end of the heating program. The light gases evolved are measured by a FT-IR gas analysis system attached directly to the heated grid cell. Details of the UTRC heated grid apparatus have been given previously (Ref. 1, 2). The power density fields in vacuum conditions consist mainly of irradiance, whereas in the presence of ambient gases there can be significant gas conduction depending on the thermal conductivity of the gas. The power density fields were determined by synchronously measuring delivered current and voltage while measuring the temperature of the screen at pseudo steady-state conditions, and normalizing with respect to screen surface area. Depending on the heat transfer and heat capacity properties of the sample relative to the screen and ambient gas, the sample can couple to the local power density field. Such coupling has been demonstrated to change the observed temperature trajectory of the screen relative to an unloaded screen area (Ref. 1, 2). The main element of interest is the magnitude of the power density levels established by the heated grid system in the 600°K to 1000°K screen temperature regime, the temperatures of tar formation and evolution in such heating systems (Refs. 3, 4, 5).

UTRC Flash Lamp (FL)

Details of the flash lamp reactor have been given previously (Ref. 6). Under the range of capacitor voltage levels used in this investigation and with the particular match of lamp characteristics and driving circuit parameters the shape of the pulse did not vary significantly. The magnitude of the irradiance level delivered to the inside of the reactor was controlled by varying the neutral density filter and/or the capacitor bank voltage levels. The real time irradiance levels of the flash pulse were monitored by fast response pyrolelectric detectors. The detectors employed were calibrated with NBS irradiance standard lamps and a NBS traceable radiometer system used in conjunction with a chopped Argon ion laser. Pyroelectric detectors have a nearly constant response to wavelength from the UV to IR spectral regimes. Because of the possibility of inducing photochemical reactions with the UV component of the flash pulse, the reactors employed were pyrex, as were the neutral density filters. The delivered radiation is characterized by wavelengths ranging from 0.4 to 2.0 microns with peak intensities between 0.8 and 1.1 microns.

Entrained Flow Reactor (EF)

In the entrained flow reactor, coal is entrained in a primary gas and injected into a hot wall furnace, through which a preheated secondary gas is flowing whose temperature is matched with the wall. Entrained coal/char particles flow in a pencil-like stream down the center of the furnace tube and

are collected by a water cooled probe. Figures 2, 3 and 4 display the overall reactor design, aerosol-char separation device and the aerosol and char separation trains. Approximately 75% of the total reactor flow is diverted to the aerosol train. Both the cyclone (char) train and impactor (aerosol) train are followed by final filters. These filters consist of porous metal disks to ease in removal of tar species. Approximately 90% of the tar mass appears to collect on the final filters, with some deposition on stages 7 and 8 of the impactor train. SEM analysis of the impactor and cyclone stages as well as the final filters reveal the phase separator extracts particulates and aerosols less than 2 microns from the particulate flow at 75% gas flow removal. Tar material deposited on the final filter substrates consists almost entirely of condensed heavy hydrocarbons having no particulate boundary structure. Particulate material is efficiently removed by the impactor and cyclone stages.

Because the coals were initially size separated by aerodynamic means, it was originally thought that the size specific ASTM ash could be used as the basis for calculating mass fraction loss via the ash tracer technique. However, using this value gave negative weight loss results for the low wall temperature runs. Inspection of the gas analysis system data and the filter stages of the cyclone and impactor trains indicated substantial devolatilization was occurring. It became apparent that the feed system was not delivering coal particles having the same average ash content as measured for the gross sample for this particular size cut. Consequently, the reactor system was operated in the cold wall, cold flow mode with the delivered coal particles collected in stage 0 of the cyclone separator considered as representative of the actually delivered samples. It was noted that immeasurably small samples of fines were deposited in the impactor train or subsequent stages of the collection system.

Tar Sampling and Handling

Tar yields in the heated grid reactor are determined by weighing the condensible material deposited on the inside of the reactor walls and filters placed between the reactor and FT-IR gas cell. Tar yields in the flash lamp reactor are defined as the THF soluble portion of the condensibles found inside the reactor and on the filters placed between the reactor and FT-IR gas cell. These tars may contain material extracted from char particles in addition to "desorbed" (vaporized molecules, ejected molecular clusters and colloidal fragments) species evolved in the flash heating process. Relative molecular weight distributions of tars were determined with the THF soluble (room temperature, ten minute ultrasonic bath) portion of the evolved species. Entrained flow reactor tars were defined as the THF soluble portion of the material removed from the filtering system. All samples were passed through a 0.5 micron filter before injection into the SEC system. The details of the SEC have been given previously (Ref. 7).

RESULTS AND DISCUSSION

Tar yields and relative molecular weight distributions were obtained for PSOC1451. The elemental analysis for the mesh and aerodynamically separated coal samples are given in Table Ia. Table Ib lists the elemental compositions observed for the 20 - 30 micron cut of the parent coal PSOC 1451 D sample, the delivered particles captured in stage 0 of the cyclone collector, and the residual particles remaining in the feeder bed after several runs. Obviously,

the feed system delivers 20 - 30 micron particles having lower average mineral densities than that observed for the gross parent sample. The residual particles, that is, the particles left in the feeder bed have higher average mineral densities than the gross parent sample. Despite the fact that the size separation system and the feeder system both employ aerodynamic principles, segregation does occur in the reactor feed process. As a result it was deemed necessary to perform cold flow runs with each sample to generate baseline ash data for determining mass raction yields by ash tracer calculations. Results for tar yields, number average (Mn), and weight average (Mw) molecular weights are summarized in Table II. The data have been arranged in order of increasing net power density. The incident power density has been estimated from reactor property measurements indicated above and heat balance calculations assuming coal particles are spherical, with emissivity and absorptivity of 0.9, and heat capacity of 0.3 cal/gm-C. The particle sizes listed are an arithmetic average diameter of the high and low cutoff of the mesh range. The entrained flow tar yields are estimates based on one atmosphere runs performed in the flash lamp and heated grid reactor where particles were heated to the same final temperatures.

The limits of the molecular weight distributions range from 100-3500 for the heated grid and entrained flow tars, and from 100-5000 for the flash lamp tars. Previous investigators have obtained similar results for average molecular weights and for the range of the MWD's of various coal tars, and coal extracts (see Table III).

Pressure Effect in a Particular Reactor

Heated grid and flash lamp experiments were conducted at atmospheric and low pressures. The entrained flow reactor was operated at one atmosphere only. Comparisons of heated grid and flash lamp data given above (Table II) reveal a highly coupled dependency between mass and heat transfer parameters in determining molecular weight characteristics of the evolved tars. Larger MWD moments are obtained with the heated grid apparatus under low pressure conditions relative to atmospheric pressure for a given power program input (Fig. 5). The low pressure tars obtained in this apparatus have a significantly larger fraction of high MW species than the corresponding atmospheric pressure tars. Tar yields are reduced by 30% or more, depending on specific conditions, while molecular weight moments are reduced. These results are consistent with the results of Unger and Suuberg (Ref. 8) and others (Ref. 9, 10).

The same MWD pattern emerges at the lowest power density inputs employed with the flash lamp apparatus. That is, the low pressure tars have significantly higher molecular weight moments than the corresponding tars formed in one atmosphere of helium or argon (Fig. 5). However, at the next highest irradiance level (285 w/cm^2) the tars formed in one atmosphere of helium have larger moments than the corresponding low pressure conditions. These results can be understood relative to the variation in heat transfer conditions. Particles subject to a radiant pulse in low pressure conditions can only cool by an ablative process whereas particles radiantly heated in the presence of an ambient gas are cooled by conduction across a boundary layer as the particle temperature rises. In low pressure conditions the tars formed within the heating particle become hot enough to undergo some secondary cracking reactions in the evolution process. Depending on its thermal conductivity, the moderating influence of the ambient gas can be appreciable,

resulting in a lowering of the net power density delivered to the particles. Consequently, the lowest irradiance level employed was not sufficient to heat the 50 micron particles, in the presence of helium, to desorb more than 5 to 10% of the coal mass as tars. In vacuum conditions, on the other hand, the observed tar yield was ~23% for the lowest irradiance level. In one atmosphere of argon the yield was ~19% with MWD moments similar but somewhat lower than the corresponding vacuum run. The results also indicate that the change in irradiance level from an average level of 225 w/cm^2 to 285 w/cm^2 in low pressure conditions results in thermal cracking reactions of the tars as they are evolving from the correspondingly hotter particles. Light gas - CH_4, CO, C_2H_2, C_2H_4, HCN-yields associated with such high temperature reactions of tars are also increased. Although increases in CH_4 and CO are observed in the heated grid gas yields when the tar evolution process is performed in pressure as opposed to vacuum, significant changes in C_2H_2 and HCN are not observed for this coal type with a change in ambient pressure alone.

Variation in Molecular Weight Distributions with Power Density Level

The influence of power density on tar yields and MWD's was explored by utilizing the multi-reactor approach discussed previously. The effect of large differences in power density is explored by comparing results from different reactors for a particular ambient gas environment (Figure 6). The heated grid tars, which were devolatilized at the lowest incident power fields are observed to have lower number average and weight average molecular weights than the flash lamp tars, devolatilized at the highest power densities. The main mode of energy transfer is radiation in these reactors when operated in low pressure conditions, although the wavelength distribution of the radiation is shifted to the visible and near IR for the flash lamp relative to the heated grid. The molecular weight moments of the entrained flow reactor tars vary substanially with residence time. In order to compare results to the other reactors, the shortest residence time tars should be examined since these presumably will have experienced the smallest degree of gas-phase secondary reactions. The tars produced in the 900^{o}C, 40 msec residence time conditions have slightly lower molecular weights than the atmospheric pressure heated grid tars while the 1000^{o}C, 40 msec tars show similar moment characteristics. In both cases the initial tars (low residence time) show molecular weight moments less than the vacuum tars formed in the heated grid. Relative to the flash lamp tars generated in either vacuum or pressure conditions the EF reactor tars have lower moment and distribution characteristics.

Devolatilization Modeling and Coal Structure

For a given set of heat transfer conditions and particle size, it can be difficult to distinguish between mass and heat transfer effects on volatiles product distributions and characteristics (Ref. 11). Both phenomena can appear to effect any one observable similarly by introducing intraparticle or extra-particle (particle-gas boundary layer or entrainment stream) secondary reactions in evolving tar species. Lumped parameter measurements - tar yield, char yield, gas yield, weight loss - are not informative and can even be misleading for a microscopic understanding of coal devolatilization. Kinetic comparisons based on one yield characteristic or product type grossly oversimplify the complexity of the process and can be even more misleading. The results reported in this investigation indicate that detailed

characteristics of tar species generated under one set of reactor conditions can give more insight into the devolatilization process, but only if careful consideration of reactor conditions are included and detailed comparisons are made to results obtained with other reactors on the same analytical bases. A combination of tar characteristics and light gas yields and composition for a wide range of reactor conditions are necessary before a comprehensive understanding of coal devolatilization can be established.

The significant change in relative MWD's of desorbed tars with heat transfer rate in low pressure conditions strongly implies a wide distribution of bonding types, ranging from predominantly physical association to covalent bonding, among a wide distribution of organic structure sizes, molecular to colloidal. The "tar" characteristics depend on the rate (power density field) at which thermal energy is delivered to the organic matrix, the mode of energy delivery and mass transport conditions. Such behavior is not unlike that exhibited by large, thermally labile organic molecules which are observed to desorb from a given substrate intact, via pyrolysis fragmentation, or in both forms, depending on the specific mass and heat transfer conditions and the nature of the molecular interactions between the adsorbed molecules and substrate (Ref. 12-19). From a devolatilization perspective high volatile bituminous coals behave as if they contain a wide range of organic structures, molecular and colloidal, attached to a polymeric-like substrate by a variety of physical and chemical bonding types. The presence of specific fractions of physically and chemically bonded species has been postulated to interpret the plastic behavior and generation of intraparticle pyridine extratables during the rapid heating of an Appalachian provide high volatile bituminous coal (4, 40). The size characteristics of the desorbed species varies depending on whether pyrolysis fragmentation or desorption of relatively large species is emphasized by the heating conditions employed in devolatilization as well as mass transport related parameters.

Acknowledgements

The authors are grateful to Dr. D. Maloney for providing tar samples for comparisons. D. Santos and G. Wagner provided critical technical assistance in carrying out this investigation. Partial funding was provided by the Department of Energy under Contract DE-AC22-84PC70768.

TABLE Ia

PSOC 1451 (HVA BIT - Appalachian Province)
Elemental Composition

Mesh	-270+325	-100+140	-50+70	-25+35	-20+25
<d>	49	127	254	604	774
%DAF					
C	82.38(0.47)*	82.26(0.36)	82.28(0.36)	80.66(2.80)	78.40(4.87)
H	5.44(0.03)	5.54(0.03)	5.58(0.02)	5.71(0.28)	5.69(0.20)
N	1.60(0.03)	1.62(0.02)	1.63(0.01)	1.56(0.08)	1.52(0.14)
S+O	10.58(0.55)	11.10(0.45)	10.48(0.37)	12.26(3.30)	14.13(4.83)
Ash	5.89(0.55)	10.78(0.69)	9.11(1.32)	24.39(18.9)	32.50(29.6)

* Numbers in parentheses represent one standard deviation.

<d> = Arithmetic average of particle range in microns

TABLE Ib

ELEMENTAL COMPOSITION OF PARENT, DELIVERED AND RESIDUAL PARTICLES:
PSOC 1451D, 20 - 30 MICRON PARTICLES

SAMPLE	%C	%H	%N	%S+O	%ASH*
PARENT-1	75.19	4.94	1.48	9.66	8.69
PARENT-2	75.25	4.95	1.45	9.52	8.80
PARENT-3	75.00	4.91	1.45	9.82	8.80
PARENT-4	75.06	4.90	1.45	9.78	8.80
DELIVERED-1	78.49	5.08	1.53	10.08	4.80
DELIVERED-2	78.54	5.08	1.50	10.36	4.50
DELIVERED-3	78.56	5.12	1.51	10.09	4.69
DELIVERED-4	78.59	5.08	1.48	10.01	4.80
RESIDUAL-1	74.46	4.91	1.41	9.49	9.69
RESIDUAL-2	74.42	4.89	1.43	9.84	9.39
RESIDUAL-3	74.45	4.90	1.45	9.99	9.19
RESIDUAL-4	74.44	4.91	1.45	9.78	9.39

TABLE II

TAR YIELDS AND MOLECULAR WEIGHTS

REACTOR/ PARAMETERS	PARTICLE SIZE [m]	ATM.	POWER DENSITY [W/CM^2]	Mn	Mw	% TAR YIELD	RUN I.D.
HG 450/2 *	49	VAC	0.62	626	839	14.2	229B
HG 550/2	49	AR	0.74	510	703	14.9	238A
HG 600/10	49	VAC	0.88	594	775	25.1	239A
HG 550/2	49	VAC	0.94	664	960	35.3	232C
HG 600/10	49	HE	1.3	522	692	12.7	242A
HG 350/1	49	VAC	1.8	655	948	20.0	224B
HG 800/2.5	49	VAC	1.9	621	855	21.0	221A
HG 800/2.5	49	VAC	1.9	610	843	24.4	237B
HG 800/2.5	254	VAC	2.0	639	869	25.1	246A
HG 800/2.5	127	VAC	2.1	616	841	28.4	245A
HG 800/2	774	VAC	2.3	616	875	24.3	253A
HG 800/2.5	774	VAC	2.3	632	869	23.3	247A
HG 800/2.5	49	AR	2.3	520	734	17.5	235C
EF 900/3 **	64	N2	50.0	485	698	****	017
EF 900/9	64	N2	-	490	709	-	018
EF 900/22	64	N2	-	382	560	-	019
EF 1000/3	64	N2	80.0	531	766	****	020
EF 1000/9	64	N2	-	406	596	-	021
EF 1000/22	64	N2	-	275	407	-	022
FL 1.8/30 ***	49	HE	225(32)	686	1059	6.0	705J
FL 1.5/60	49	HE	285(40)	784	1184	12.0	703C
FL 1.5/90	49	HE	430(60)	699	1134	19.0	704B
FL 2.2/60	49	HE	730(96)	545	898	17.0	706E
FL 1.8/30	49	AR	225(122)	714	1121	19.0	707C
FL 1.8/30	49	VAC	225	764	1180	23.0	709B
FL 1.5/60	49	VAC	285	663	1054	28.4	713B
FL 2.2/60	49	AR	729(293)	630	955	22.0	708B

Footnotes:

* HG X/Y - heated grid with 1000 C/sec ramp to X C, hold for Y sec, then 1000° C/sec ramp to 800°C, hold for 2.5-Y sec. The 600/10 runs are an exception: ramp to 600°C and hold for 10 sec.

** EF X/Y - entrained flow with X C gas temperature and Y" sampling position
900°C: 3"- 40 msec; 9" - 110 msec; 22" - 250 msec
1000°C: 3"- 40 msec; 9" - 100 msec; 22" - 230 msec

*** FL X/Y - flash lamp with X KV capacitor bank voltage and Y% neutral density filter. Values are time-averaged delivered irradiance; values inside parentheses are time-averaged net power density calculated from heat balance considerations. See Table III for characteristics of flash pulses.

***** - Not measured directly; at 3" residence time is estimated be about 20% (daf) of the parent coal mass from heated grid and flash lamp investigations. This yield represents the major fraction of the total volatile yields (Ref. 25) in 40 msec.

TABLE III

COMPARISON OF MOLECULAR WEIGHTS OF COAL DERIVED COMPOUNDS

SAMPLE	TECHNIQUE	Mn	Mw	MWD RANGE	INVESTIGATOR(S)
Pitt #8	SEC THF				this work
1 atm HG tar		500-525	675-750	100-3500	
vac HG tar		575-675	775-975	100-3500	
EF tar		275-550	400-775	100-3500	
1 atm FL tar		550-800	900-1200	100-5000	
vac FL tar		650-775	1050-1200	100-5000	
Pitt #8	SEC/VPO pyridine				Oh (1985)
HG tars:					
1 atm		350	-	100-1200	
vac		400	-	100-1200	
HG char extracts:					
1 atm		450	-	100-1500	
vac		500	-	100-1500	
Pitt Bruceton	SEC/VPO THF				Unger & Suuberg (1984)
HG tars:					
1 atm		500-700	-	100-4000	
vac		750-900	-	100-4000	
HG 1 atm char extracts:		750-1000	-	100-4000+	
Pitt #8 CO2 laser	SEC				Ballantyne et al. (1983)
1 atm tar	THF	223?	394?	60-3000	
Low Beam Shaw 84.2% C 115°C pyridine raw coal extract	Ebullio-scopy pyridine	870	-	-	Dormans & van Krevelen (1960)

REFERENCES

1. Freihaut, J.D., Zabielski, M.F. and Seery, D.J., Nineteenth Symposium (Int'l.) on Combustion, The Combustion Institute, 1159 (1982).

2. Freihaut, J.D. and Seery, D.J., ACS Div. of Fuel Chem., Preprints, 27, No. 2, 89 (1982).

3. Howard, J.B. in Chemistry of Coal Utilization, Sec. Supp. Vol. (ed. by Elliott, M.A.), John Wiley and Sons, New York, 340ff (1981).

4. Fong, W.S., Khalil, Y.F., Peters, W.A. and Howard, J.B., Fuel, 65, 195 (1986).

5. Suuberg, E.M., et al., Seventeenth Symposium (Int'l.) on Combustion, The Combustion Institute, Pittsburgh, 117 (1979).

6. Freihaut, J.D. and Seery, D.J., Proceedings of the International Conference on Coal Science, IEA, 957 (1985).

7. Freihaut, J. D., Proscia, W. M. and Seery, D. J. Proceedings of the Third Annual Pittsburgh Coal Conference, 684 (1986).

8. Unger, P.E., and Suuberg, E.M., Fuel, 63, 606 (1984).

9. Oh, M.S., Ph.D. Thesis, M.I.T., Cambridge, MA, 1985.

10. Solomon, P.R., Squire, K.R., and Carangelo, R.M., Proceedings of the International Conference on Coal Science, IEA, 945 (1985).

11. Kaiser, M., Wanzl, W., van Heek, K.H. and Juntgen, H., Proceedings of the International Conference on Coal Science, IEA, 899 (1985).

12. Cotter, R.J., Analytical Chemistry, 52, No. 14, 1589A.

13. Van der Peyl, G.J.Q., Haverkamp, J. and Kistemaker, P.G., Internat. Jnl. of Mass Spectrometry and Ion Physics, 42, 125 (1982).

14. Beuhler, R.J., Flanigan, E., Greene, L.J. and Friedman, L., J. Amer. Chem. Society, 96, No. 12, 3990 (1974).

15. Heresch, F., Schmid, E.R. and Huber, J.F.K., Anal. Chem., 52, 1803 (1980).

16. Posthumus, M.A., Kistemaker, P.G. and Meuzelaar, H.L.C., Analytical Chemistry, 50, No. 7, 985 (1978).

17. Cotter, R.J., Analytical Chemistry, 52, 1770 (1980).

18. Stoll, R. and Rollgen, F.W., Org. Mass. Spec., 14, No. 12, (642) (1979).

19. Kistemaker, P.G., Lens, M.M.J., Van der Peyl, G.J.Q., and Boerboon, A.J.H., Adv. in Mass Spectrometry, 8A, 928 (1980).

Fig. 1 Reactor Heat Transfer Regimes

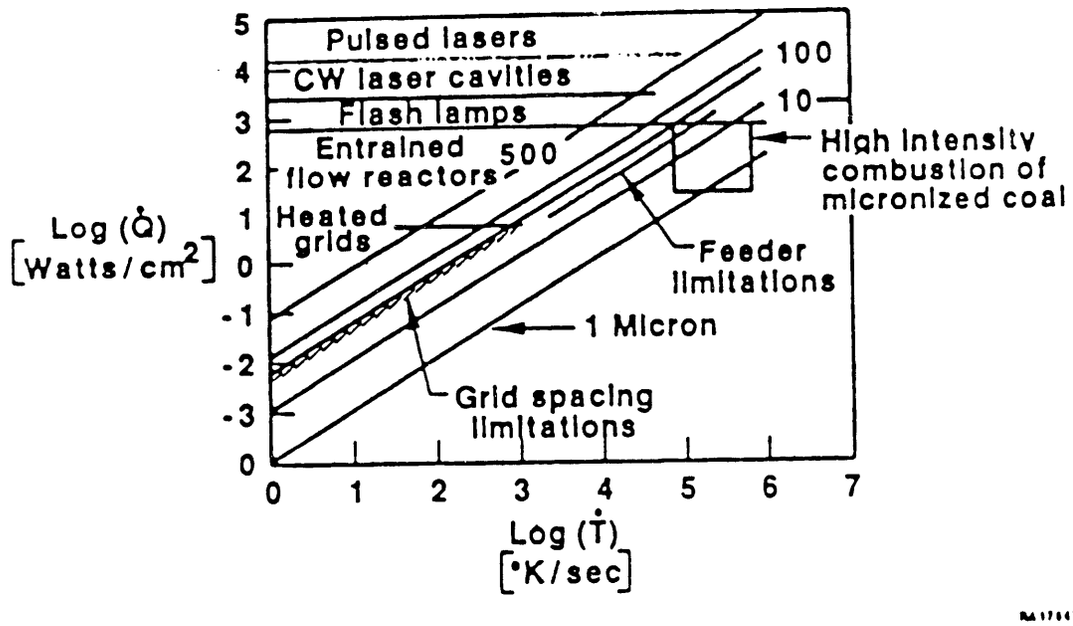

FIGURE 2

ENTRAINED FLOW REACTOR FOR COAL DEVOLATILIZATION

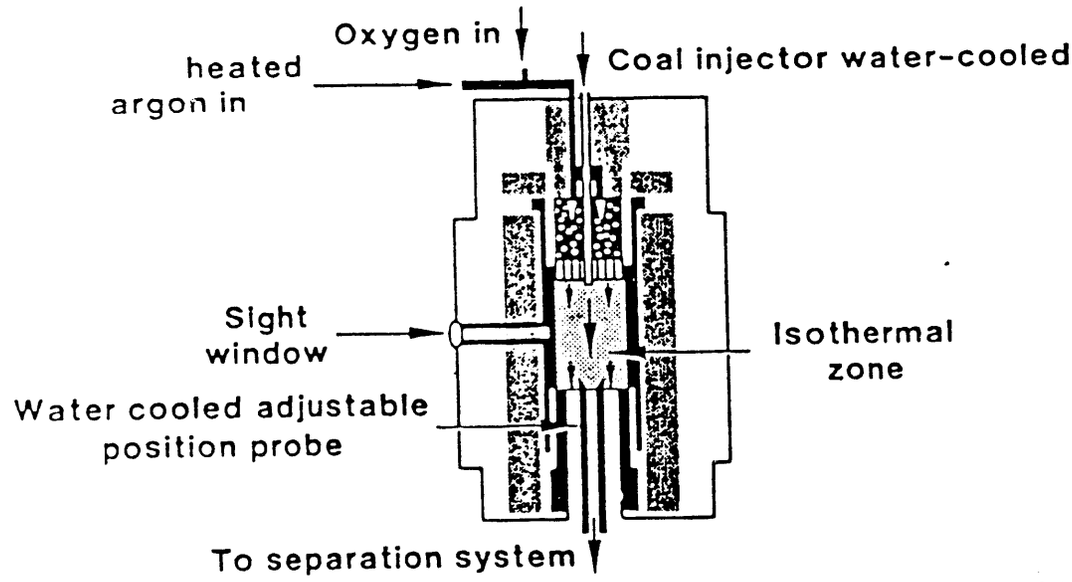

FIGURE 3

AEROSOL - CHAR SEPARATION APPARATUS

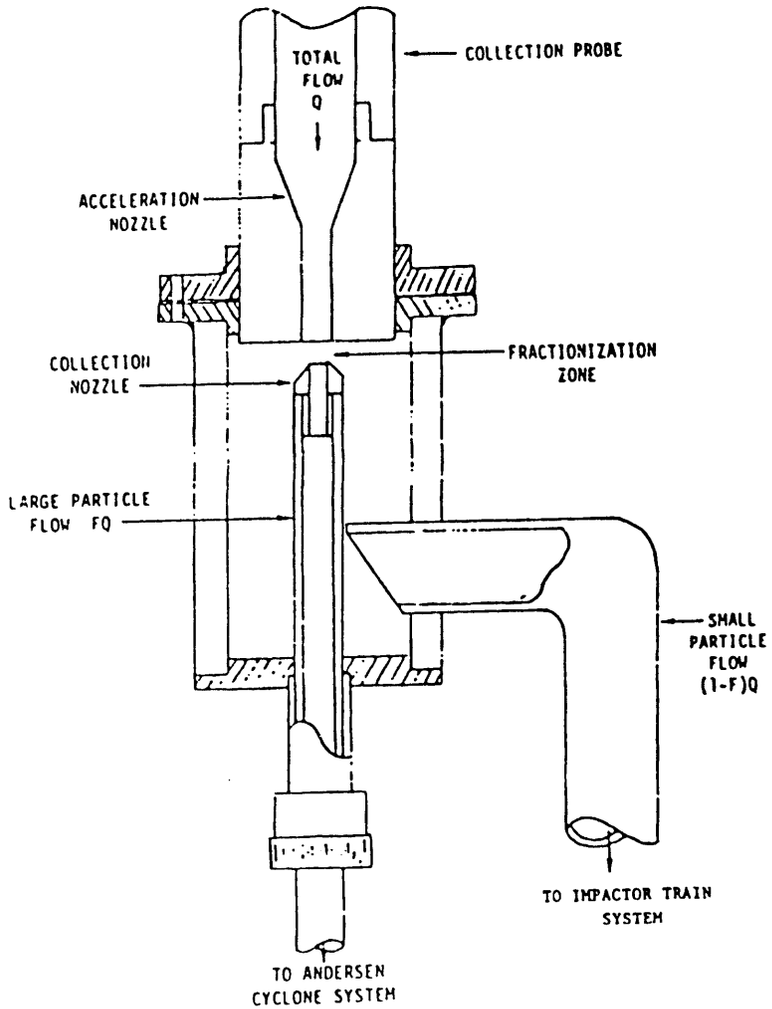

FIGURE 4

SAMPLE COLLECTION SYSTEM

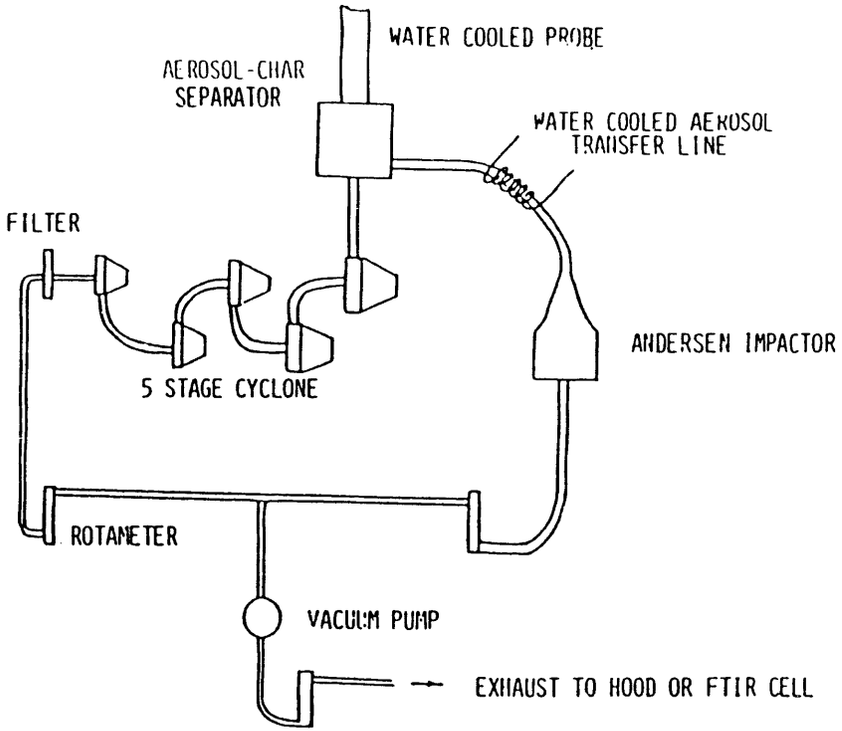

FIG. 5

EFFECT OF PRESSURE

On tar molecular weight distributions

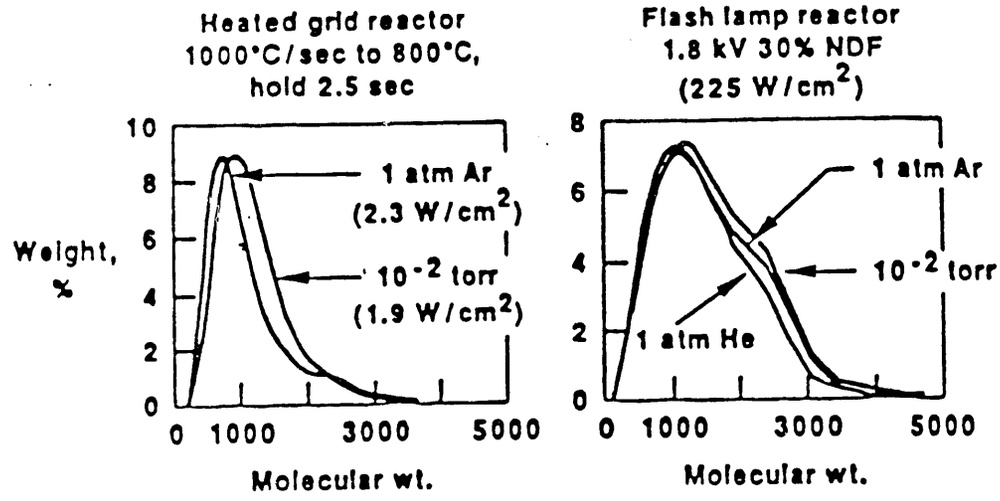

FIG. 6

EFFECT OF DIFFERENT REACTORS

On tar molecular weight distributions

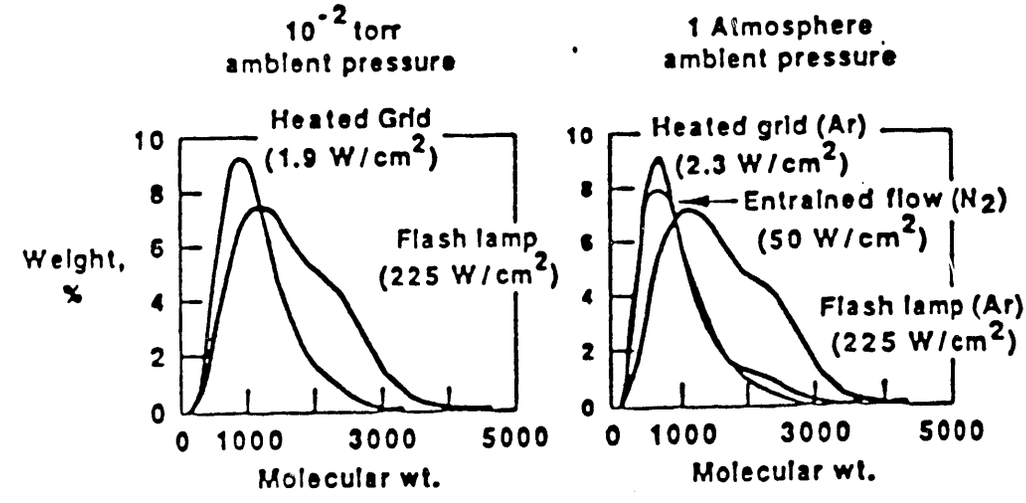

END

DATE FILMED

11/13/91